Nitric Oxide 102 (2020) 1–11

Contents lists available at ScienceDirect

Nitric Oxide

journal homepage: www.elsevier.com/locate/yniox

Total body irradiation-induced colon damage is prevented by nitrate-mediated suppression of oxidative stress and homeostasis of the gut microbiome

Weili Wang[a,b,1], Liang Hu[a,c,1], Shimin Chang[a,d], Linsha Ma[a,d], Xiangchun Li[a,e], Zi Yang[a], Conglin Du[a], Xingmin Qu[a], Chunmei Zhang[a,g], Songlin Wang[a,f,g,*]

[a] Salivary Gland Disease Center and Beijing Key Laboratory of Tooth Regeneration and Function Reconstruction, Capital Medical University School of Stomatology, Beijing, China
[b] Department of Stomatology, Aerospace Center Hospital, Beijing, China
[c] Outpatient Department of Oral and Maxillofacial Surgery, School of Stomatology, Capital Medical University, Beijing, China
[d] Department of Stomatology, Beijing Friendship Hospital, Capital Medical University, Beijing, China
[e] Department of Stomatology, The First Hospital of Qinhuangdao, Qinhuangdao, China
[f] Department of Biochemistry and Molecular Biology, Capital Medical University School of Basic Medicine, Beijing, China
[g] Immunology Research Center for Oral and Systemic Health, Beijing Friendship Hospital, Capital Medical University, Beijing, China

ARTICLE INFO

Keywords:
Nitrate
Total body irradiation
Colonic mucosa
Oxidative stress injury
Gut microbiome

ABSTRACT

Inorganic dietary nitrate plays vital roles in biological functions via the exogenous NO_3^-/NO_2^-/NO pathway under hypoxia and ischemia. We previously verified the antioxidative effects of inorganic nitrate in a mouse model of total body irradiation (TBI). Accordingly, in this study, we evaluated the effects of inorganic nitrate on prevention of TBI-induced colon injury and dysbiosis of the gut microbiome. Nitrate significantly rescued the abnormal biological indexes (body weight, white blood cell, red blood cell, platelet, hemoglobin level and intestinal canal lengths) induced by TBI. Then, we detected oxidative stress and DNA damage indexes (phosphohistone H2AX and p53 binding protein 1), which were both increased by irradiation (IR) and alleviated by nitrate. IR-induced apoptosis and senescence were ameliorated by inorganic nitrate. The distribution of the gut microbiome differed for mice with TBI and those receiving inorganic nitrate. The average abundance of Lactobacillus significantly increased, and that of Bacteroidales decreased at the genus level in the nitrate group compared with that in the IR alone group. At 30 days after TBI, the abundances of Bacteroides and Faecalibaculum decreased, whereas that of Lactobacillus increased in the IR + nitrate group compared with that in the IR alone group. Inorganic nitrate efficiently prevents TBI-induced colon epithelium injury and maintains the homeostasis of the gut microbiome. Thus, our results showed that inorganic nitrate might be a promising treatment for TBI induced colon injury.

1. Introduction

Radiotherapy is commonly used in the treatment of tumors. Total body irradiation (TBI) is performed prior to hematopoietic stem cell transplantation in patients with adult T cell leukemia [1]. Various complications occur with TBI, including interstitial pneumonitis and other toxicities [2]. Despite attempts to reduce the side effects of TBI, systemic damage is still observed in clinical treatment.

Excess reactive oxygen species (ROS) are produced after exposure to radiation, causing chronic oxidative damage in various organs [3,4]. Oxidative stress induced by ROS accumulation is a major mechanism leading to apoptosis following DNA damage [5]. Moreover, ROS accumulation results in decreased self-renewal and stress-induced cell death in stem cell senescence biology [6].

The gut microbiome composition differs among individuals and is influenced by multiple genetic and environmental factors, including diet, drugs, age, and health [7,8]. Dysbiosis of the gut microbiota is associated with many gastrointestinal diseases [9]. Radiation

* Corresponding author. Salivary Gland Disease Center and Beijing Key Laboratory of Tooth Regeneration and Function Reconstruction, Capital Medical University School of Stomatology, Tian Tan Xi Li No.4, Beijing, 100050, China.
E-mail address: slwang@ccmu.edu.cn (S. Wang).
[1] Weili Wang and Liang Hu contribute equally in this study.

https://doi.org/10.1016/j.niox.2020.05.002
Received 4 February 2020; Received in revised form 12 May 2020; Accepted 13 May 2020
Available online 26 May 2020

enteropathy involves acute and chronic gastrointestinal side effects [10], and the abundance of pathogenic bacteria is generally increased in these diseases. Additionally, radiotherapy influences the gut microbiome and dysbiotic bacteria, thereby aggravating gastrointestinal symptoms [11,12].

Under hypoxic and ischemic conditions, NOS-derived nitric oxide (NO) is inhibited, and nitrate-nitrite-NO pathway is facilitated [13]. Inorganic nitrate supplementation increases exogenous NO and plays vital biological functions [14]. Additionally, salivary nitrate secretion and nitrite formation are increased, protecting the gastric mucosa against stress-induced injury via the NO pathway [15]. Notably, the diversity and pathology of the oral microbiota influence the nitrate/nitrite/NO pathway [16]. However, the relationships between nitrate and the microbiome are still unclear.

It was reported that TBI causes DNA injury at an early stage in multiple organs and that dietary nitrate effectively alleviates the resulting systemic damage in mice [17]. Here, we evaluated whether inorganic nitrate prevents TBI-induced colon injury. Our results provide important insights into the protective effects of inorganic nitrate in alleviating TBI-induced colon injury.

2. Materials and methods

2.1. Application and detection of nitrate in animals

Nitrate ($NaNO_3$; cat. no. S8170; Sigma-Aldrich, Germany), dissolved with pure water to a concentration of 2 mM, was applied 1 week before receiving TBI and continued to 30 days after TBI. Part of the colon was collected and weighed. The tissues were homogenized, and nitrate and nitrite concentrations were detected according to standard procedures using a Total Nitric Oxide and Nitrate/Nitrite Parameter Assay Kit (cat. no. PKGE001; R&D Systems, USA).

2.2. Immunofluorescence and immunohistochemistry

Samples embedded in OCT were sectioned into 10-μm-thick sections and blocked with blocking buffer (cat. no. ab126587; Abcam, USA). Samples were then incubated with primary antibodies targeting phospho-H2AX (1:250; cat. no. ab22551; Abcam) and p53 binding protein 1 (53BP-1; 1:200; cat. no. ab131442; Abcam) at 4 °C overnight, followed by incubation with secondary anti-mouse antibodies for phospho-H2AX (1:500; Alexa Fluor 594; cat. no. ab150120; Abcam) and secondary anti-rabbit antibodies for 53BP-1 (1:500; Alexa Fluor 488; cat. no. ab150073; Abcam) at room temperature for 1 h. Sections were then photographed using a confocal system and digital camera (SP8; Leica, Weztlar, Germany). At least three fields in each section and five different sections were used for calculations.

Samples were fixed with neutral formalin, embedded in paraffin, and sectioned (5 μm thickness). After dehydration with graded alcohol and antigen retrieval, sections were blocked and incubated with antibodies targeting p53 (1:500; cat. no. ab188224; Abcam) or endogenous nitric oxide synthase (eNOS; 1:1000; cat. no. ab76198; Abcam), followed by incubation with secondary antibodies (1:300; cat. no. ab7090; Abcam) for 1 h at 26 °C. Sections were observed using an Olympus BX51 microscope (Olympus Corporation, Japan) and photographed using Image Pro Plus 6.0. At least three fields in each section and five different sections were used for calculations.

2.3. Western blotting and quantitative real-time reverse transcription polymerase chain reaction (qRT-PCR)

Proteins were extracted using RIPA buffer containing protease (cat. no. P1265; Applygen, Technologies, Inc., China) and phosphatase inhibitors (cat. not. P1260; Applygen). Proteins were separated on polyacrylamide gels and then transferred to membranes. The membranes were incubated with primary antibodies targeting phospho-H2AX (1:1000; cat. no. ab22551; Abcam), superoxide dismutase (SOD) 2 (1:2000; cat. no. ab13534; Abcam), p21 (1:1000; cat. no. ab188224; Abcam), eNOS (1:1000; cat. no. ab76198; Abcam), caspase3 (1:1000; cat. no. 9662; Cell Signaling Technology, USA), and p53 (1:1000; cat. no. ab131442; Abcam) overnight at 4 °C. The membranes were then incubated with secondary antibodies (1:1000; cat. no. ab7090; Abcam) for 1 h at 26 °C. The protein bands were detected using a Bio-Rad ChemiDoc MP (Bio-Rad, Hercules, CA, USA) and Image Lab 3.0 system. The analyses were repeated three times, and data were calculated using Image J Pro Plus 6.0.

For qRT-PCR, total RNA was extracted from colon tissues using SYBR Green (cat. no. DP431; Tiangen Biotech, Beijing, China), and reverse transcription was carried out using a Fastquant RT Super Mix Kit (cat. no. KR108; Tiangen Biotech). Primers are listed in Supplementary Table 1. The real-time PCR mixture (primer, cDNA and single-stranded RNA) was prepared, and PCR was carried out using a CFX96 Real-Time System (Bio-Rad) as previously reported [18].

2.4. ROS detection and terminal deoxynucleotidyl transferase dUTP nick-end labeling (TUNEL) assays

Fresh samples without fixation were frozen and embedded in OCT. The samples were sectioned at 10-μm thickness. Using a ROS Fluorescein Assay Kit (cat. no. GMS10016.6; Genmed Scientifics, Inc., USA), sections were stained at room temperature and incubated at 37 °C for approximately 20 min. Next, the sections were stained with 4′,6-diamidino-2-phenylindole and observed by confocal laser scanning microscopy (TCS SP8; Leica). We evaluated five different sections and three fields in each section. Image Pro Plus 6.0 was used for quantification of ROS. We first calculated the average fluorescence intensity of ROS and nuclear. Then, we used the ratio of ROS versus nuclear to show the change of ROS in this study.

Apoptosis levels were detected using TUNEL staining. Briefly, samples were fixed, embedded in paraffin, sectioned, stained, and observed by confocal laser scanning microscopy (TCS SP8; Leica). We evaluated five different sections and three fields in each section. The TUNEL-positive area was calculated using Image Pro Plus 6.0.

2.5. Blood sample collection and blood routine examination

After animals were anesthetized, blood samples were collected from the ophthalmic vein and evaluated immediately at the School of Stomatology, Capital Medical University using standard hematology procedures. White blood cells (WBCs), red blood cells (RBCs), platelets (PLTs), and hemoglobin (HGB) were examined.

2.6. Fecal sample collection and 16S RNA examination

Animals were sacrificed from day 7 to day 30 after TBI. Fecal samples were directly collected from the lower segment of the colon. The samples were then stored at −80 °C and examined by Biomarker Technologies (Beijing, China).

Feces from the normal and inorganic nitrate groups (n = 6) were collected on day 0. Samples from the irradiation (IR) and IR + inorganic nitrate (IR + Nit) groups (n = 6) were collected on days 7 and 30 after TBI. Genomic DNA was extracted and quantified. PCR products were tested by electrophoresis and quantified using a QuantiFluor-ST system. Using an Illumina HiSeq sequence platform and paired-end method, microbiome diversity was detected. According to operational taxonomic unit analysis, the detected microbiome was separated and analyzed at different levels of classification using α diversity, the Ace index (reflecting the richness), and the Shannon and Simpson indexes (reflecting the diversity). The most abundant species from six groups were selected. Nonmetric multidimensional scaling (NMDS) was used to simplify the samples or variables to low-dimensional space, and subsequent analyses were then carried out. The

original relationships between objects were preserved. Linear discriminant analysis effect size (LEfSe) was used to show the significant biomarkers among groups. 16S functional gene analysis was performed using PICRUSt software, and Kyoto Encyclopedia of Genes and Genomes (KEGG) analyses were carried out to determined differences and changes in metabolic pathways of functional genes.

2.7. Statistical analysis

Data are presented as means ± standard errors of the means and analyzed using SPSS 19.0. Results with p values of less than 0.05 were considered significant. Charts and figures were generated using GraphPad 6.0 and Photoshop CS6, respectively. Shapiro-Wilk normalized tests and homogeneity of variance tests were performed before using one-way analysis of variance and Bonferroni post-hoc tests to compare differences among groups for data with normal distributions and equal variance. Kruskal-Wallis tests and Mann-Whitney U tests were used for data with non-normal distributions or unequal variance.

3. Results

3.1. Recovery of the general condition of mice by nitrate treatment

The experiment design is shown in Supplementary Fig. 1. Mouse weight increased with time. The tendencies in the normal control, inorganic nitrogen, and IR + Nit groups were similar, although weight gain in the IR group was much slower than that in the other groups. On day 30 after TBI, the weight in the IR group was significantly lower than that in the other three groups (Fig. 1A). Moreover, changes in WBC, RBC, PLT, and HGB concentrations were similar in the IR and IR + Nit groups. The abnormal index recovered to almost normal by day 30 after TBI. However, significant decreases in WBC levels at 4 h, RBC levels at 7 days, PLT levels at 2 and 4 h, and HGB levels at 24 h and 7 days were observed in the IR group compared with that those in the IR + Nit group (Fig. 1B–E). The length of the intestinal canal was shortened at 6 and 24 h after TBI and partially recovered on days 7 and 30 (Supplementary Fig. 2). The intestinal canal length was significantly shorter in the IR group than in the normal control group, whereas no significant differences were observed between the IR and IR + Nit groups (Fig. 1F).

3.2. Oxidative stress and DNA damage were alleviated in the IR + Nit group

Oxidative stress is decreased in the submandibular gland and lungs after nitrate supplementation [17]. Here, we measured ROS levels in the colon at various times after TBI. ROS levels increased after TBI and peaked at 24 h. At 4 h, 6 h, and 7 days, ROS levels in the IR + Nit group were decreased compared with those in the IR group (Fig. 2A, C). ROS subsequently induced DNA damage and increased apoptosis in both normal and cancer cells [19]. Analysis of phospho-H2AX and 53BP-1 levels at 2, 4, 6, and 24 h after TBI by immunofluorescence showed that DNA damage gradually increased, peaking at approximately 6–12 h after TBI. In contrast, phospho-H2AX levels were significantly decreased in the IR + Nit group compared with those in the IR group (Fig. 2B, D). 53BP-1 levels in the IR + Nit group were also decreased

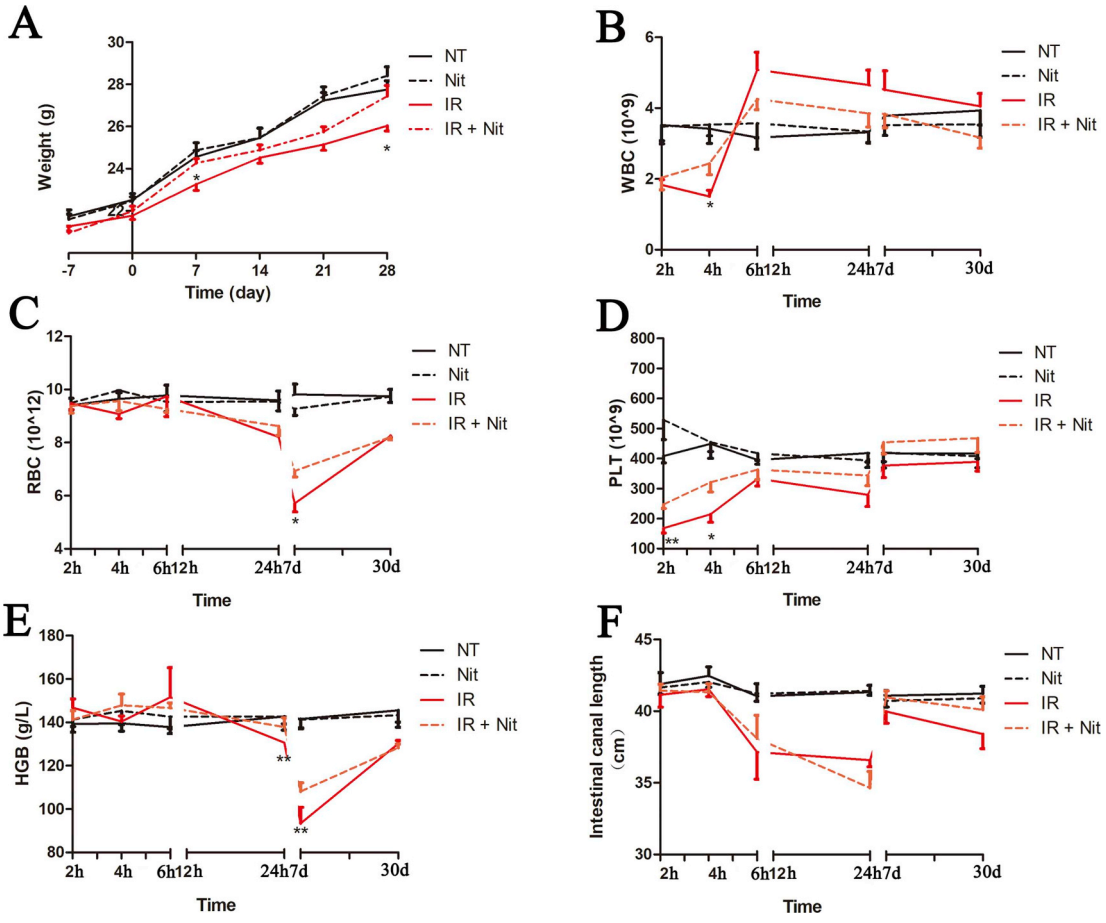

Fig. 1. Nitrate recovered TBI-induced abnormalities in general condition.
Body weights of mice in the four groups (A). WBCs (B), RBCs (C), PLTs (D), and HGB concentrations (E) in the four groups. Intestinal canal length was calculated (F). Data are presented as means ± SEMs (n = 6 mice/group). *p < 0.05, **p < 0.01.

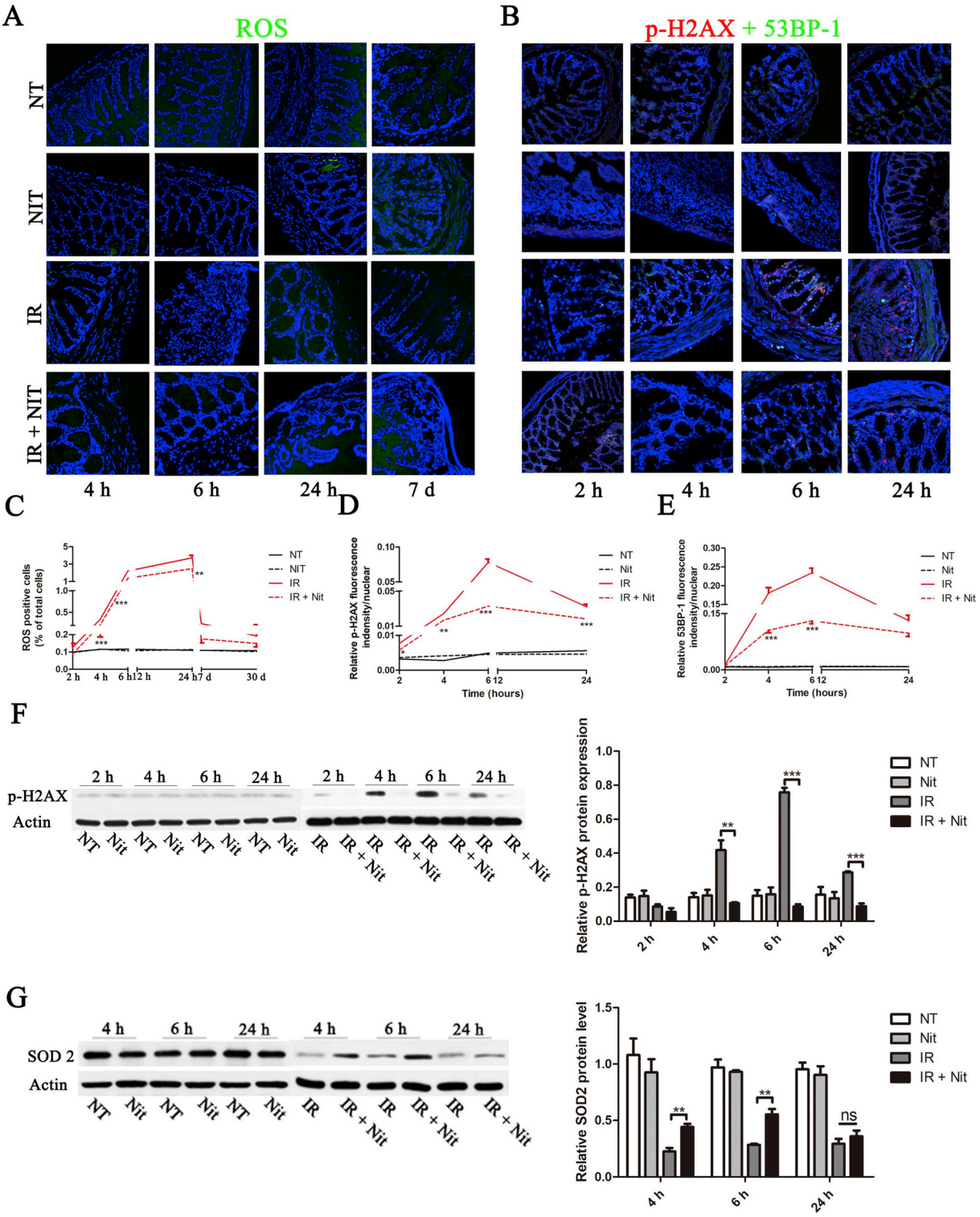

Fig. 2. Nitrate alleviated the increased oxidative stress induced by TBI.
ROS expression was detected using immunofluorescence analysis (A, C). Phospho-H2AX and 53BP-1 levels after TBI (B, D, E). Western blotting was used to detect changes in phospho-H2AX (F) and SOD2 protein levels (G). Data are shown as means ± SEMs. $*p < 0.05$, $**p < 0.01$, $***p < 0.001$. Three fields were evaluated from each of five sections per sample. Western blotting was repeated independently three times.

compared with those in the IR group at 4 and 6 h after TBI (Fig. 2B, E). Moreover, western blotting for detection of phospho-H2AX confirmed the reduced DNA damage in the nitrate group. At 4, 6, and 24 h after TBI, phospho-H2AX levels in the IR + Nit group were decreased compared with those in the IR group (Fig. 2F). Notably, SOD2 expression was decreased after TBI, but significantly recovered in the IR + Nit group compared with that in the IR group (Fig. 2G).

3.3. Nitrate slightly inhibited apoptosis after TBI

Apoptosis is a mechanism of programmed cell death tightly regulated by caspase proteases [20]. Therefore, we evaluated caspase 3

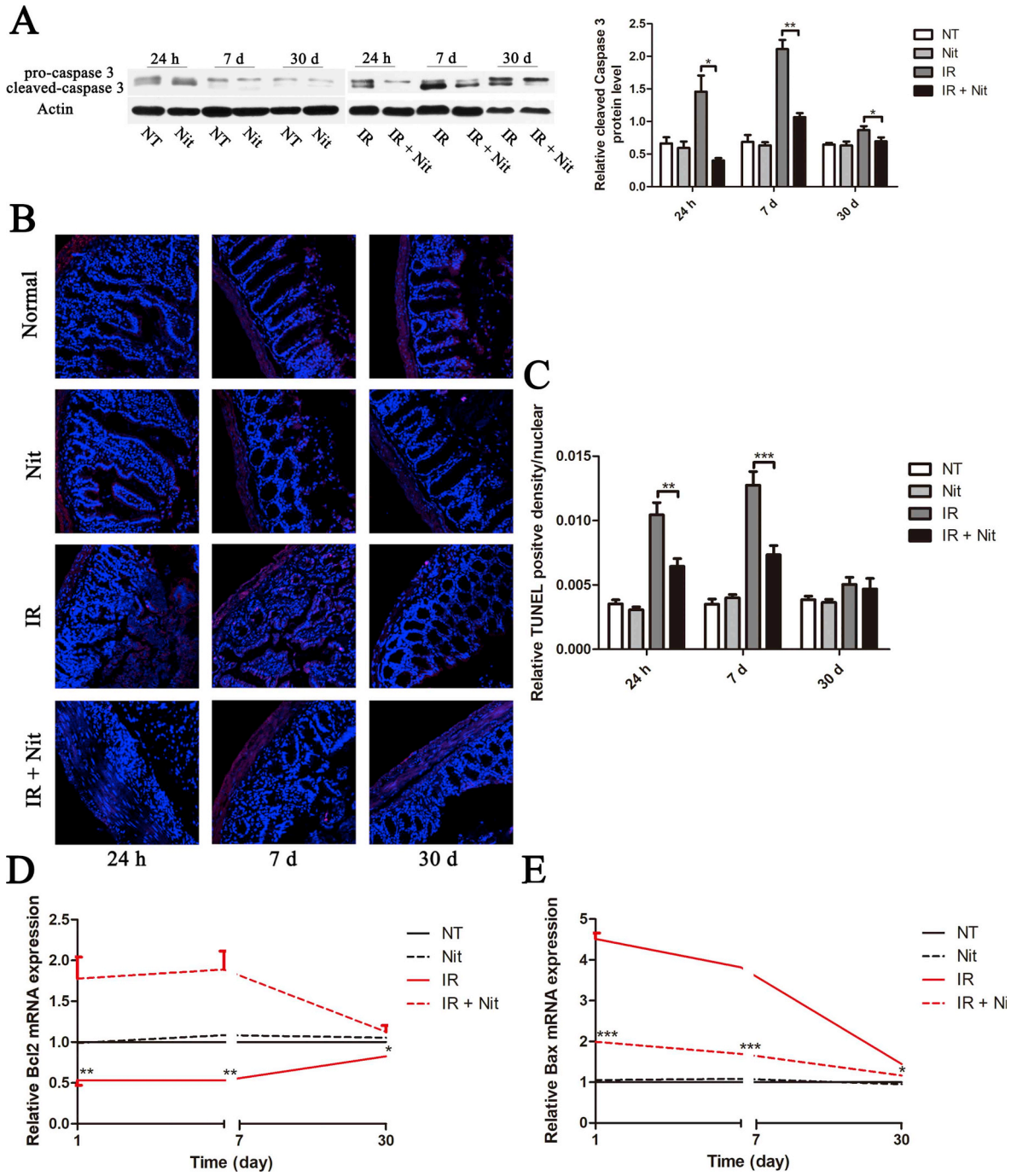

Fig. 3. Nitrate blocked TBI-induced apoptosis.
Cleaved caspase 3 levels at 24 h, 7 days, and 30 days after TBI (A). TUNEL staining was performed to show apoptosis levels (B, C). *Bcl-2* and *Bax* mRNA levels were evaluated by PCR (D, E). Data are shown as means ± SEMs. $*p < 0.05$, $**p < 0.01$, $***p < 0.001$. Three fields were evaluated from each of five sections per sample. Western blotting and PCR were repeated independently three times.

expression after TBI. Cleaved caspase 3 expression was increased in the IR group and significantly decreased in the IR + Nit group (Fig. 3A). Moreover, nitrate significantly alleviated TBI-induced apoptosis in the colon. In contrast, on day 30, no significant differences were found among groups (Fig. 3B and C).

The apoptotic pathway is regulated by the Bcl-2 protein family and the Bcl-2/Bax ratio [21]. Thus, we evaluated *Bcl-2* and *Bax* mRNA levels. Notably, *Bax* expression was significantly increased after TBI, although decreased expression was observed in the IR + Nit group compared with that in the IR group. The opposite changes were observed for *Bcl-2* expression (Fig. 3D).

3.4. Nitrate recovered TBI-induced senescence in the colon

IR inhibits cell cycle progression in human mesenchymal stem cells and induces senescence by activating the p53 pathway [22]. Moreover, IR-induced senescence caused long-term damage by preventing the renewal of tissues progenitor cells [23]. In our study, we found that p53 and p21 protein levels were significantly increased at 2, 4, and 6 h after receiving TBI, and nearly complete recovery was observed at 24 h. Notably, the increase in p53 expression was blocked in the IR + Nit group compared with that in the IR group (Fig. 4A and B). Western blotting showed that nitrate alleviated senescence by decreasing p53

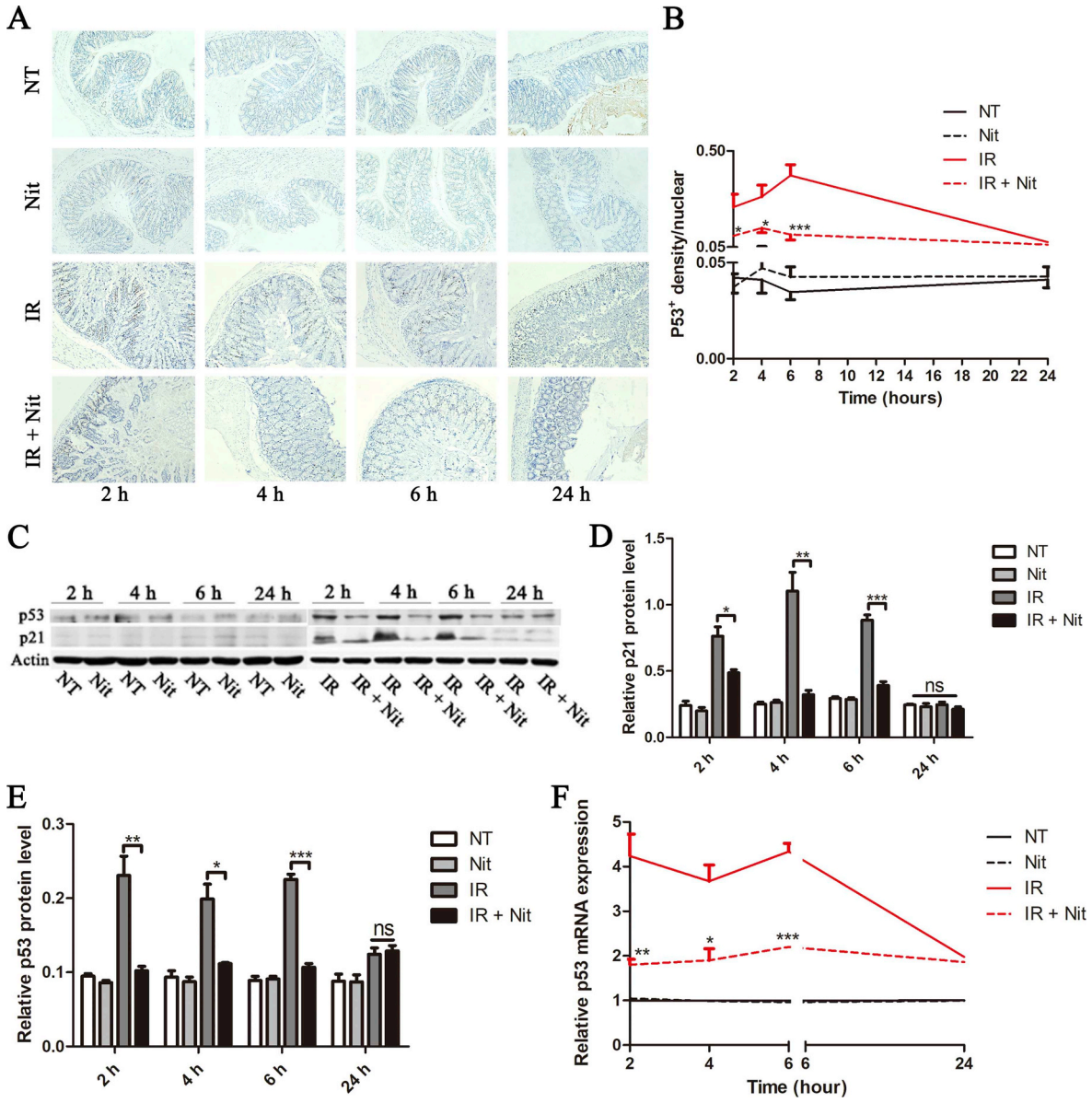

Fig. 4. Nitrate blocked TBI-induced senescence.
p53 protein expression was detected by immunohistochemistry and western blotting (A–C, E). p21 protein expression (D). Changes in *p53* mRNA levels were evaluated by PCR (F). Data are shown as means ± SEMs. $^{*}p < 0.05$, $^{**}p < 0.01$, $^{***}p < 0.001$. Three fields were evaluated from each of five sections per sample. Western blotting and PCR were repeated independently three times.

and p21 levels at 2, 4, and 6 h after TBI (Fig. 4C–E). Moreover, *p53* mRNA was significantly decreased in the IR + Nit group compared with that in the IR group (Fig. 4F). Thus, the anti-senescence function of nitrate was speculated associated with the inhibition of the p53 senescence pathway.

We collected multiple organs as heart, liver, spleen, lung, kidney and observed the histological change with or without IR/nitrate. Results showed that no significant change was found among those groups in our presented data (Supplementary Fig. 3).

3.5. The $NO_3^-/NO_2^-/NO$ pathway was activated in the IR + Nit group

Beneficial effects of inorganic nitrite was reported in model using activated immune cells and nitrite attenuated iNOS activation and oxidative stress [24]. Here, we found that the nitrite concentration in colon homogenates in the IR group tended to decrease compared with that in the normal control group at 2, 4, 6, and 24 h, although the differences were not significant. In contrast, at 7 and 30 days after TBI, nitrite concentrations were significantly reduced in the IR group. In both the inorganic nitrogen and IR + Nit groups, nitrite concentrations were increased. However, on days 7 and 30 after TBI, nitrite concentrations were decreased in the IR + Nit group (Fig. 5A).

Additionally, cGMP levels began to decrease at 2 h; cGMP concentrations in the IR + Nit group were significantly higher at 6 h, 24 h, 7 days, and 30 days after TBI (Fig. 5B). Moreover, eNOS protein expression decreased after IR and was then partially recovered in the IR + Nit group (Fig. 5C–E).

3.6. Nitrate regulated the abnormal gut microbiome after TBI

The gut microbiome plays vital roles in regulating abnormal conditions [25]. Accordingly, we analyzed the gut microbiota on days 7 and 30 after TBI. There were no significant differences in α-diversity among groups (Supplementary Fig. 4). However, NMDS results showed

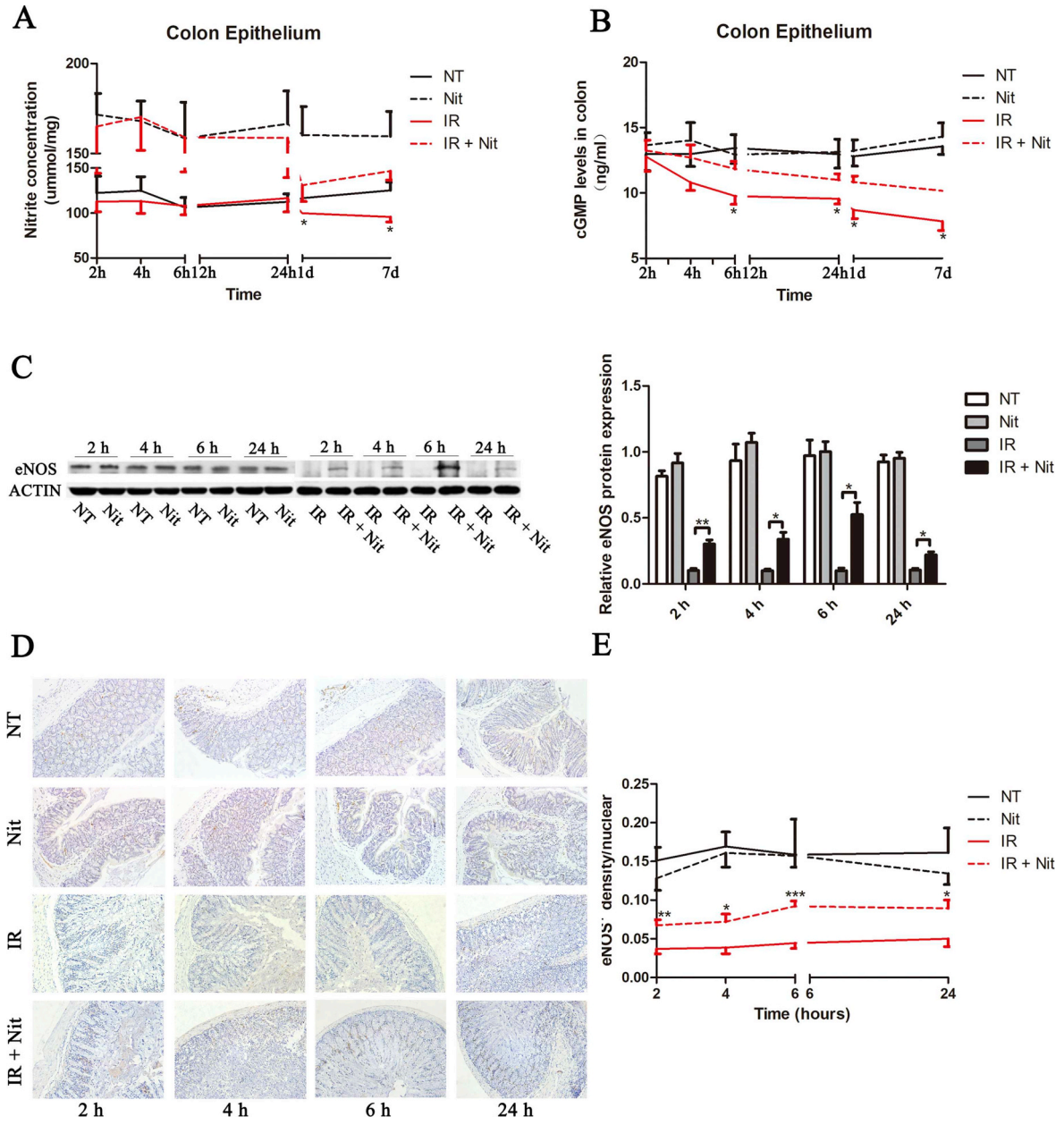

Fig. 5. Inorganic nitrate activated the $NO_3/NO_2/NO$ pathway.
Nitrite concentrations in the four groups (A). cGMP levels in the colon (B). eNOS protein levels were detected using western blotting (C) and immunohistochemistry (D, E). Data are shown as means ± SEMs. *$p < 0.05$, **$p < 0.01$, ***$p < 0.001$. Three fields were evaluated from each of five sections per sample. Western blotting was repeated independently three times.

that after receiving TBI, the gut microbiome in mice changed. Intriguingly, at day 30 after IR, the distributions of the gut microbiome in the IR and IR + Nit groups were different from those in the normal control group and were separated from each other (Fig. 6A).

The major species identified in these groups were *uncultured_bacterium_f_Bacteroidales_S24-7_group*, *Lactobacillus*, *Ruminococcaccae_UCG-014*, *Lachnospiraceae_NK4A136*, *Prevotellaceae_UCG-001*, *Akkermansia*, *Bacteroides*, *uncultured_bacterium_f_Lachnospiraceae*, *Alistipes*, *Alloprevotella*, and *Eubacterium_coprostanoligenes_group*. The average richness of *Bacteroidales_S24-7_group* in the IR group was increased compared with that in the normal control group at 30 days, whereas the richness decreased in the IR + Nit group at 30 days. The abundance of *Akkermansia* was increased in the IR and IR + Nit groups at 30 days, whereas Ruminococcaceae _UCG-014 was increased in the IR + Nit group at 30 days (Fig. 6B). The ratio of Firmicutes/Bacteroidetes in IR 30d group significantly decreased compared with NT group, IR 7d and IR + Nit 30d group (Supplementary Fig. 5).

LEfSe showed that no different bacteria were found between the normal control and IR groups at 7 days, indicating that the gut microbiome did not change significantly at 7 days after IR. However, on day 30 after IR, the abundance of *Alloprevotella* and *Firmicutes* was decreased, whereas that of *uncultured_Bacteroidales_S24-7_group*, *Bacteroidales_S24-7_group*, *Akkermansia*, and *Verrucomicrobiaceae* was increased in the IR group compared with that in the IR group at 30 days (Fig. 6C). Moreover, *Bacteroides* and *Bacteroidaceae* abundance was increased in the IR group on day 7 compared with that in the IR + Nit group on day 7 (Fig. 6D). On day 30 after IR, nitrate supplementation increased the abundance of *Firmicutes*, *Bacillus*, *Lactobacillales*, *uncultured_Lactobacillus*, *Lactobacillaceae*, *Lactobacillus*, and *Ruminococcaceae_UCG_014*, whereas the abundance of *Rikenellaceae*, *Butyricimonas*,

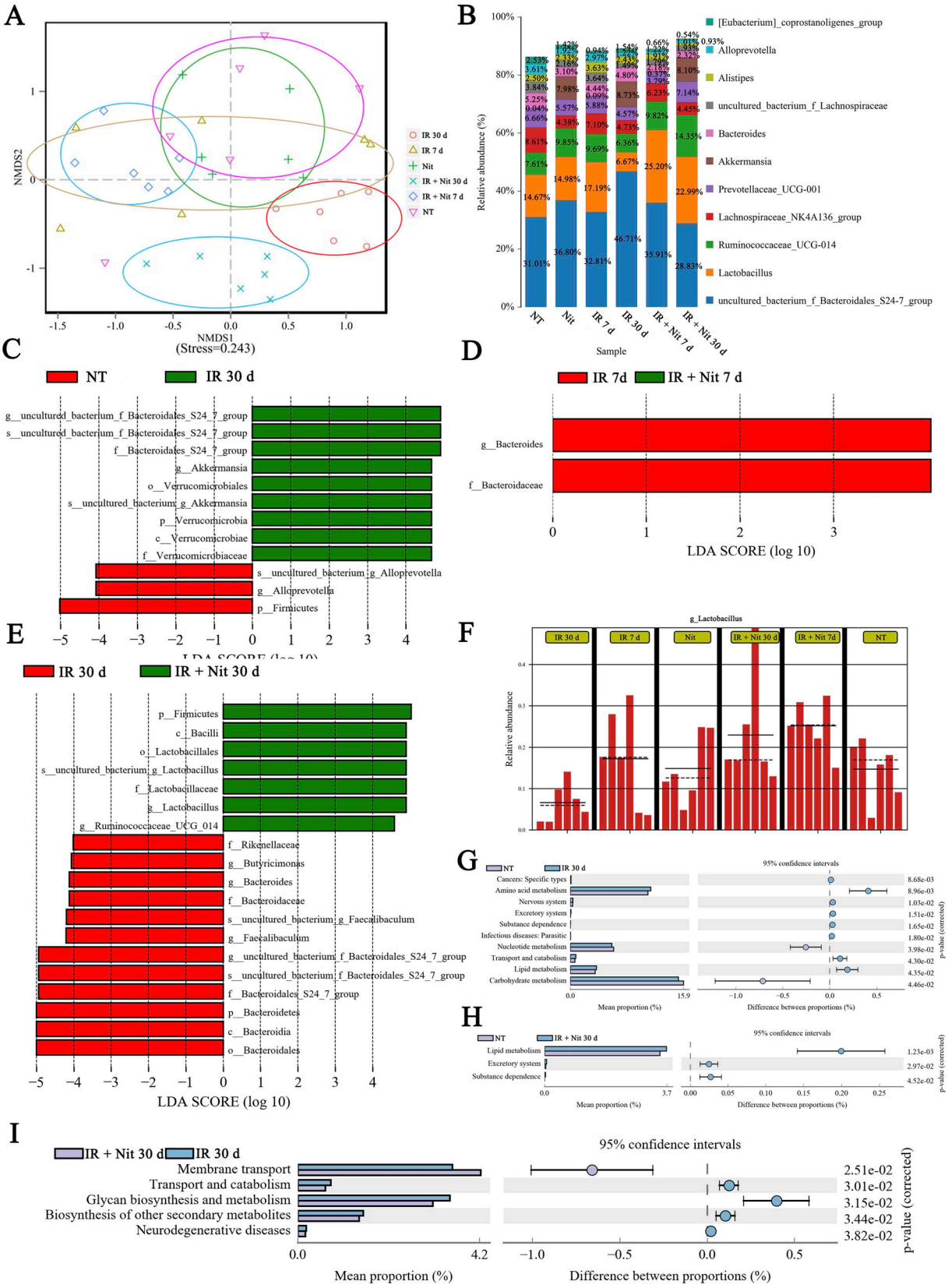

Fig. 6. The analysis of gut microbiome among four groups.
NMDS analysis of the microbiome in the four groups (A). Relative abundances of the major microbial groups at the genus level (B). Abundances of different bacteria after IR for 30 days (C) and 7 days with or without nitrate (D). Abundances of multiple bacteria in the IR + Nit and IR groups at 30 days (E). Relative abundances of *Lactobacillus* in all six groups (F). Significant KEGG pathways between the normal control (NT) and IR groups at 30 days, the NT and IR + Nit groups at 30 days, and the IR and IR + Nit groups at 30 days (G–I). Six samples were evaluated in each group.

Bacteroides, *Bacteroidaceae*, *uncultured_Faecalibaculum*, *Faecalibaculum*, and *uncultured_Bacteroidales_S24_7_group* was increased in the IR group on day 30 (Fig. 6E). The relative abundance of *Lactobacillus* in all six groups increased significantly in the IR + Nit group (Fig. 6F).

Gene function analysis using the KEGG database showed that there were no significant differences between the NT and IR groups on day 7. The pathways of cancers, infectious diseases, and lipid metabolism were upregulated in the IR group on day 30, whereas the pathways of nucleotide metabolism and carbohydrate metabolism were downregulated compared with those in the NT group (Fig. 6G). The pathways of lipid metabolism, excretory system, and substance dependence were upregulated in the IR + Nit group on day 30 compared with those in the NT group, similar to those in the IR group on day 30 (Fig. 6H). Moreover, the gene functions of transport and catabolism, glycan biosynthesis and metabolism, biosynthesis of other secondary metabolites, and neurodegenerative diseases were upregulated in the IR group compared with those in the IR + Nit group on day 30. In contrast, the pathway of membrane transport, process by which ions and solutes pass through the membrane was downregulated in the IR group at 30 days (Fig. 6I), indicating that the gut bacteria-released LPS-like compounds could easier to enter the circulation.

4. Discussion

Inorganic dietary nitrate alleviates TBI-induced lung and submandibular gland injury by decreasing DNA damage [17]. Here, we observed the preventive effects of inorganic dietary nitrate on TBI-induced colon injury. Our results demonstrated the protective effects of nitrate on physiology and the gut microbiome following TBI in mice.

IR induces ROS accumulation and increases oxidative stress and tissue injury [26,27]. ROS and DNA damage induced by IR then cause multiple systemic problems [18,28]. Increased ROS accumulation also decreases bioactive NO levels during the early reperfusion phase [29,30]. NO signaling could reduce the expression of ROS in cardiomyocytes by posttranslational mitochondrial complex I modification [31]. Indeed, in a mouse model of TBI, nitrate had anti-oxygenation effects in the submandibular gland and lungs [17]. Moreover, inorganic nitrate attenuated IR-induced oxidative stress by upregulating SOD2, which leads to reduced ROS accumulation, suggesting that nitrate may promote the deacetylation of Mn-SOD [32].

In our study, indexes of phospho-H2AX and 53BP-1, which are associated with DNA damage [33], were increased in the colon epithelium after TBI and decreased in the IR + Nit group, indicating the protective effects of inorganic nitrate on alleviation of DNA damage. Senescence is a state in which cells lose their ability to proliferate, synthesize DNA, and divide [34]. Our results showed that inorganic nitrate inhibited IR-induced senescence by downregulating p21 and p53. Moreover, apoptosis was decreased in the nitrate group. Thus, inorganic nitrate efficiently mitigated IR-induced DNA damage, senescence, and apoptosis.

In various metabolic disorders, exogenous synthesis of NO is reduced, and the $NO_3/NO_2/NO$ pathway is inhibited [14,35]. Moreover, eNOS knockout causes hypertension, dyslipidemia, insulin resistance, and visceral adipose tissue accumulation in mice [36–38]. Thus, impairment of the $NO_3/NO_2/NO$ pathway may be important for these metabolic diseases. Here, we verified downregulation of the $NO_3/NO_2/NO$ pathway and showed that exogenous dietary nitrate upregulated the $NO_3/NO_2/NO$ pathway after TBI, indicating that dietary nitrate could efficiently rescue impaired NO production occurring under pathological conditions. Thus, we hypothesized that $NO_3/NO_2/NO$ pathway activation may be a key mechanism through which nitrate prevented IR-induced colon injury.

The gut microbiome plays vital roles in human health, and imbalance of the gut microbiome results in chronic immune-mediated diseases, such as inflammatory bowel disease and colitis-associated colorectal cancer [39]. In our study, the gut microbiome did not change significantly at 7 days after IR; however, at 30 day after IR obvious changes in bacteria were observed. Notably, there were no differences in α-diversity among all six groups, indicating that both IR and nitrate could alter the gut microbiota slightly. However, the NMDS results showed that the distribution of the gut microbiome at day 30 after IR was distinct from that in the normal control group. The distributions of gut microbiota in the IR and IR + Nit groups were also distinct. Overall, our results showed that nitrate could regulate the abnormal microbiome induced by IR.

The gut microbiome and human health are reciprocally related [40]. Most organisms in the gut microbiome showed similar genus levels among the six groups. The increased abundance of *Bacteroidales_S24-7_group*, *Akkermansia*, and Ruminococcaceae could have functions in relieving high-fat diet-induced weight gain [41]. In this study, our gut microbiome analysis results showed that the abundance of *uncultured_Bacteroidales_S24-7_group* was increased in the IR group and decreased in the IR + Nit group at 30 days, which could partially explain the recovered body weight after nitrate supplementation. Moreover, the abundance of *Lactobacillus*, which could enhance epithelial barrier function via nuclear factor-κB and mitogen-activated protein kinase pathways [42], was increased after Nit treatment. We hypothesized that the biological functions of inorganic nitrate may be related to increased abundance of *Lactobacillus*.

Lactobacillus abundance was increased in the IR + Nit group at 7 and 30 days, but did not increase following treatment with Nit alone. The exogenous $NO_3/NO_2/NO$ pathway was not activated under normal conditions. However, in hypoxic and ischemic conditions, which block NO production, this $NO_3/NO_2/NO$ pathway is activated [24,43]. Although this phenomenon could partially explain the changes observed in *Lactobacillus*, the mechanisms are still unclear, and additional studies are required.

In this study, we found no differences in the microbiome between the normal control and IR groups at 7 days. However, at 30 days after IR, *Bacteroidales_S24-7_group*, *Akkermansia*, and *Verrucomicrobiaceae* abundance was increased, whereas *Alloprevotella* and *Firmicutes* abundance was decreased compared with those in the normal control group. The changes in *Bacteroidales_S24-7_group* and *Firmicutes* abundance partially explained the decreased body weights observed after receiving TBI [44]. Abundance of *Akkermansia*, which was negatively associated with rheumatoid arthritis, atherosclerosis, and dyslipidemia [45], was increased in the TBI group, verifying the efficient clinical application of TBI for the treatment of patients undergoing multiple stem cell transplantations [46]. Short-chain fatty acids, which influence the maintenance of gut and immune homeostasis [47], are related to the abundance of *Alloprevotella* and *Lactobacillus*. Abundance of *Verrucomicrobiaceae*, which is associated with Parkinson's disease [48], was increased in the IR group at 30 days.

In the nitrate group, the increased abundance of *Firmicutes* partially explained the recovered body weight [44]. *Bacillus* provides numerous benefits in human health [49] and was increased in the nitrate group. Moreover, the abundance of *Lactobacillus*, which is typically considered a beneficial bacterium [50], was significantly increased after nitrate supplementation. In contrast, compared with that in the IR + Nit group, the abundance of *Rikenellaceae*, which has been reported to be associated with the severity of systemic lupus erythematosus [51], and *Butyricimonas*, which shows increased abundance in patients with hepatocellular carcinoma [52], both increased in the IR group. ROS are positively correlated with *Bacteroides* and *Faecalibaculum*, and SOD is positively related to *Lactobacillus* [53]. The abundance of *Bacteroides* and *Faecalibaculum* in the IR group was increased, and the richness of *Lactobacillus* was decreased compared with that in the IR + Nit group, explaining the reduced oxidative stress after nitrate supplementation. Consistent with these findings, we showed that TBI induced upregulation of genes related to cancers, infectious diseases, and lipid metabolism, indicating the potentially damaging effects of TBI on the general health of experimental animals. Interestingly, aberrant NO pathways

have been implicated in multiple neurological disorders [54], and IR + Nit blocked upregulation of genes related to the neurodegenerative disease pathway.

The dosage used in TBI ranged from 2 to 8 Gy in one to four fractions, and variations in dose can result in different consequences [55,56]. In this study, 5-Gy TBI was relatively safe and only caused mild injury. Moreover, both beneficial and pathogenic gut microbes were altered in the IR group at 30 days compared with that in the normal control group. In contrast, in the IR + Nit group, the enriched microbiome mostly included beneficial bacteria or those negatively related to oxidative stress, explaining the decreased oxidative stress observed in the nitrate group.

In conclusion, the present study showed that inorganic nitrate could partially attenuated TBI-induced colon injury. Oxidative stress was significantly alleviated, and IR-induced senescence and apoptosis were blocked by nitrate treatment. The abundance of *Bacteroides* and *Faecalibaculum* was decreased, whereas that of *Lactobacillus* [53] was increased in the IR + Nit group. However, the mechanisms through which nitrate regulates the microbiome are not clear, and additional studies are required. Thus, our findings showed that inorganic nitrate had multiple beneficial effects and may be a promising therapeutic strategy for IR-induced injury.

Author contributions

SW designed and supported the experiment. WLW and LH performed most of the experiment and wrote the manuscript. SMC, LSM, XCL, LYJ, XMQ and CMZ contributed to the samples and data collection.

Declaration of competing interest

The authors declare no conflicts of interest.

Acknowledgement

This study was supported by grants from National Natural Science Foundation of China (91649124) and School excellent doctoral thesis advisor support project of Capital Medical University (0900-19000202); Chinese Academy of Medical Sciences Research Unit (No. 2019RU020), Capital Medical University; Beijing Municipal Science & Technology Commission No.Z181100001718208; Beijing Municipal Education Commission No. 119207020201; and grants from Beijing Municipality Government (Beijing Scholar Program- PXM2018_014226_000021, PXM2017_014226_000023, PXM2018_193312_000006_0028S643_FCG and SML20151401).

Appendix A. Supplementary data

Supplementary data to this article can be found online at https://doi.org/10.1016/j.niox.2020.05.002.

References

[1] M. Tanaka, Y. Kawazu, T. Yoshida, T. Konishi, N. Takenouchi, M. Miwa, Effects of radiation based on whole-body irradiation in HTLV-1-infected mice, J. Radiat. Res. 60 (5) (2019) 710–713.

[2] Y. Chiang, C.H. Tsai, S.H. Kuo, C.Y. Liu, M. Yao, C.C. Li, S.Y. Huang, B.S. Ko, C.T. Lin, H.A. Hou, W.C. Chou, J.H. Liu, C.C. Lin, S.J. Wu, S.C. Hsu, Y.C. Chen, K.H. Lin, D.T. Lin, H.T. Chou, M.Y. Lu, Y.L. Yang, H.H. Chang, M.C. Liu, X.W. Liao, J.K. Wu, S.C. Chou, C.L. Cheng, C.Y. Chen, W. Tsay, H.F. Tien, J.L. Tang, Y.H. Chen, Reduced incidence of interstitial pneumonitis after allogeneic hematopoietic stem cell transplantation using a modified technique of total body irradiation, Sci. Rep. 6 (2016) 36730.

[3] A. Rezaie, R.D. Parker, M. Abdollahi, Oxidative stress and pathogenesis of inflammatory bowel disease: an epiphenomenon or the cause? Dig. Dis. Sci. 52 (2007) 2015–2021.

[4] D.D. New, K. Block, B. Bhandhari, Y. Gorin, H.E. Abboud, IGF-I increases the expression of fibronectin by Nox4-dependent Akt phosphorylation in renal tubular epithelial cells, Am. J. Physiol. Cell Physiol. 302 (2012) C122–C130.

[5] D.A. Chistiakov, I.A. Sobenin, V.V. Revin, A.N. Orekhov, Y.V. Bobryshev, Mitochondrial aging and age-related dysfunction of mitochondria, BioMed Res. Int. 2014 (2014) 238463.

[6] F. Chen, Y. Liu, N.K. Wong, J. Xiao, K.F. So, Oxidative stress in stem cell aging, Cell Transplant. 26 (2017) 1483–1495.

[7] S. Ahmadmehrabi, W.H.W. Tang, Gut microbiome and its role in cardiovascular diseases, Curr. Opin. Cardiol. 32 (2017) 761–766.

[8] C. Human, Microbiome Project, Structure, function and diversity of the healthy human microbiome, Nature 486 (2012) 207–214.

[9] M.R. Ferreira, A. Muls, D.P. Dearnaley, H.J. Andreyev, Microbiota and radiation-induced bowel toxicity: lessons from inflammatory bowel disease for the radiation oncologist, Lancet Oncol. 15 (2014) e139–e147.

[10] M. Reis Ferreira, J. Andreyev, K. Mohammed, L. Truelove, S.M. Gowan, J. Li, S.L. Gulliford, J. Marchesi, D.P. Dearnaley, Microbiota and radiotherapy-induced gastrointestinal side-effects (MARS) study: a large pilot study of the microbiome in acute and late radiation enteropathy, Clin. Canc. Res. 25 (21) (2019) 6487–6500.

[11] A. Lavrinienko, T. Mappes, E. Tukalenko, T.A. Mousseau, A.P. Moller, R. Knight, J.T. Morton, L.R. Thompson, P.C. Watts, Environmental radiation alters the gut microbiome of the bank vole Myodes glareolus, ISME J. 12 (2018) 2801–2806.

[12] D. Casero, K. Gill, V. Sridharan, I. Koturbash, G. Nelson, M. Hauer-Jensen, M. Boerma, J. Braun, A.K. Cheema, Space-type radiation induces multimodal responses in the mouse gut microbiome and metabolome, Microbiome 5 (2017) 105.

[13] E. Weitzberg, J.O. Lundberg, Novel aspects of dietary nitrate and human health, Annu. Rev. Nutr. 33 (2013) 129–159.

[14] L. Ma, L. Hu, X. Feng, S. Wang, Nitrate and nitrite in health and disease, Aging Dis. 9 (2018) 938–945.

[15] L. Jin, L. Qin, D. Xia, X. Liu, Z. Fan, C. Zhang, L. Gu, J. He, I.S. Ambudkar, D. Deng, S. Wang, Active secretion and protective effect of salivary nitrate against stress in human volunteers and rats, Free Radic. Biol. Med. 57 (2013) 61–67.

[16] C.D. Koch, M.T. Gladwin, B.A. Freeman, J.O. Lundberg, E. Weitzberg, A. Morris, Enterosalivary nitrate metabolism and the microbiome: intersection of microbial metabolism, nitric oxide and diet in cardiac and pulmonary vascular health, Free Radic. Biol. Med. 105 (2017) 48–67.

[17] S. Chang, L. Hu, Y. Xu, X. Li, L. Ma, X. Feng, J. Wang, C. Zhang, S. Wang, Inorganic nitrate alleviates total body irradiation-induced systemic damage by decreasing reactive oxygen species levels, Int. J. Radiat. Oncol. Biol. Phys. 103 (2019) 945–957.

[18] L. Hu, Z. Zhu, B. Hai, S. Chang, L. Ma, Y. Xu, X. Li, X. Feng, X. Wu, Q. Zhao, L. Qin, J. Wang, C. Zhang, F. Liu, S. Wang, Intragland Shh gene delivery mitigated irradiation-induced hyposalivation in a miniature pig model, Theranostics 8 (2018) 4321–4331.

[19] A. Wiseman, Oxygen-induced reperfusion-injury is caused by ROS: amelioration is possible by recombinant-DNA antioxidant enzymes and mimics in selected tissues, Med. Hypotheses 66 (2006) 329–331.

[20] M.Y. Yao, J. Zhang, S.Q. Guo, X.L. Bai, Z.H. Li, X. Zhou, Liraglutide inhibits the apoptosis of human nucleus pulposus cells induced by high glucose through PI3K/Akt/caspase-3 signaling pathway, Biosci. Rep. 39 (8) (2019) BSR20190109.

[21] C. Zhang, Y. Yu, Q. Huang, K. Tang, SIRT6 regulates the proliferation and apoptosis of hepatocellular carcinoma via the ERK1/2 signaling pathway, Mol. Med. Rep. 20 (2019) 1575–1582.

[22] K. Kurpinski, D.J. Jang, S. Bhattacharya, B. Rydberg, J. Chu, J. So, A. Wyrobek, S. Li, D. Wang, Differential effects of x-rays and high-energy 56Fe ions on human mesenchymal stem cells, Int. J. Radiat. Oncol. Biol. Phys. 73 (2009) 869–877.

[23] O.N.L. Le, F. Rodier, F. Fontaine, J.P. Coppe, J. Campisi, J. DeGregori, C. Laverdiere, V. Kokta, E. Haddad, C.M. Beausejour, Ionizing radiation-induced long-term expression of senescence markers in mice is independent of p53 and immune status, Aging Cell 9 (2010) 398–409.

[24] T. Yang, M. Peleli, C. Zollbrecht, A. Giulietti, N. Terrando, J.O. Lundberg, E. Weitzberg, M. Carlstrom, Inorganic nitrite attenuates NADPH oxidase-derived superoxide generation in activated macrophages via a nitric oxide-dependent mechanism, Free Radic. Biol. Med. 83 (2015) 159–166.

[25] J. Halfvarson, C.J. Brislawn, R. Lamendella, Y. Vazquez-Baeza, W.A. Walters, L.M. Bramer, M. D'Amato, F. Bonfiglio, D. McDonald, A. Gonzalez, E.E. McClure, M.F. Dunklebarger, R. Knight, J.K. Jansson, Dynamics of the human gut microbiome in inflammatory bowel disease, Nat. Microbiol. 2 (2017) 17004.

[26] A.F. Soliman, M. Saif-Elnasr, S.M.A. Fattah, Platelet-rich plasma ameliorates gamma radiation-induced nephrotoxicity via modulating oxidative stress and apoptosis, Life Sci. 219 (2019) 238–247.

[27] K. Kawamura, F. Qi, J. Kobayashi, Potential relationship between the biological effects of low-dose irradiation and mitochondrial ROS production, J. Radiat. Res. 59 (2018) ii91–ii97.

[28] Q. Hou, M. Wang, S. Wu, X. Ma, G. An, H. Liu, F. Xie, Oxidative changes and apoptosis induced by 1800-MHz electromagnetic radiation in NIH/3T3 cells, Electromagn. Biol. Med. 34 (2015) 85–92.

[29] C. Penna, D. Mancardi, R. Rastaldo, P. Pagliaro, Cardioprotection: a radical view Free radicals in pre and postconditioning, Biochim. Biophys. Acta 1787 (2009) 781–793.

[30] J.L. Zweier, M.A. Talukder, The role of oxidants and free radicals in reperfusion injury, Cardiovasc. Res. 70 (2006) 181–190.

[31] M. Totzeck, U.B. Hendgen-Cotta, T. Rassaf, Nitrite-nitric oxide signaling and cardioprotection, Adv. Exp. Med. Biol. 982 (2017) 335–346.

[32] M.R. Sultana, P.K. Bagul, P.B. Katare, S. Anwar Mohammed, R. Padiya, S.K. Banerjee, Garlic activates SIRT-3 to prevent cardiac oxidative stress and mitochondrial dysfunction in diabetes, Life Sci. 164 (2016) 42–51.

[33] R.F. Ferreira, D.R. Souza, A.S. Souza, Factors that induce DNA damage involving

histone H2AX phosphorylation, Radiology 277 (2015) 307–308.
[34] S. Wang, Q. Wang, H. Wang, C. Qin, X. Cui, L. Li, Y. Liu, H. Chang, Induction of ROS and DNA damage-dependent senescence by icaritin contributes to its antitumor activity in hepatocellular carcinoma cells, Pharm. Biol. 57 (2019) 424–431.
[35] M. Siervo, S.J. Jackson, L.J.C. Bluck, In-vivo nitric oxide synthesis is reduced in obese patients with metabolic syndrome: application of a novel stable isotopic method, J. Hypertens. 29 (2011) 1515–1527.
[36] M. Carlstrom, F.J. Larsen, T. Nystrom, M. Hezel, S. Borniquel, E. Weitzberg, J.O. Lundberg, Dietary inorganic nitrate reverses features of metabolic syndrome in endothelial nitric oxide synthase-deficient mice, Proc. Natl. Acad. Sci. U. S. A. 107 (2010) 17716–17720.
[37] P.L. Huang, eNOS, metabolic syndrome and cardiovascular disease, Trends Endocrinol. Metabol. 20 (2009) 295–302.
[38] S. Cook, O. Hugli, M. Egli, P. Vollenweider, R. Burcelin, P. Nicod, B. Thorens, U. Scherrer, Clustering of cardiovascular risk factors mimicking the human metabolic syndrome X in eNOS null mice, Swiss Med. Wkly. 133 (2003) 360–363.
[39] M. Kang, A. Martin, Microbiome and colorectal cancer: unraveling host-microbiota interactions in colitis-associated colorectal cancer development, Semin. Immunol. 32 (2017) 3–13.
[40] A.C. Ericsson, A.R. Personett, G. Turner, R.A. Dorfmeyer, C.L. Franklin, Variable colonization after reciprocal fecal microbiota transfer between mice with low and high richness microbiota, Front. Microbiol. 8 (2017) 1–13.
[41] L. Zhao, Q. Zhang, W.N. Ma, F. Tian, H.Y. Shen, M.M. Zhou, A combination of quercetin and resveratrol reduces obesity in high-fat diet-fed rats by modulation of gut microbiota, Food Funct. 8 (2017) 4644–4656.
[42] S. Lebeer, J. Vanderleyden, S.C.J. De Keersmaecker, Genes and molecules of lactobacilli supporting probiotic action, Microbiol. Mol. Biol. Rev. 72 (2008) 728-+.
[43] L.S. Ma, L. Hu, X.Y. Feng, S.L. Wang, Nitrate and nitrite in health and disease, Aging Dis. 9 (2018) 938–945.
[44] A. Koliada, G. Syzenko, V. Moseiko, L. Budovska, K. Puchkov, V. Perederiy, Y. Gavalko, A. Dorofeyev, M. Romanenko, S. Tkach, L. Sineok, O. Lushchak, A. Vaiserman, Association between body mass index and Firmicutes/Bacteroidetes ratio in an adult Ukrainian population, BMC Microbiol. 17 (2017).
[45] N. Shi, S. Zhang, G. Silverman, M. Li, J. Cai, H. Niu, Protective effect of hydroxychloroquine on rheumatoid arthritis-associated atherosclerosis, Anim. Model Exp. Med. 2 (2019) 98–106.
[46] S. Eder, J. Canaani, E. Beohou, M. Labopin, J. Sanz, W. Arcese, R. Or, J. Finke, A. Cortelezzi, D. Beelen, J. Passweg, G. Socie, G. Gurman, M. Aljurf, M. Stelljes, S. Giebel, M. Mohty, A. Nagler, Thiotepa-based conditioning versus total body irradiation as myeloablative conditioning prior to allogeneic stem cell transplantation for acute lymphoblastic leukemia: a matched-pair analysis from the Acute Leukemia Working Party of the European Society for Blood and Marrow Transplantation, Am. J. Hematol. 92 (2017) 997–1003.
[47] J. Tan, C. McKenzie, M. Potamitis, A.N. Thorburn, C.R. Mackay, L. Macia, The role of short-chain fatty acids in health and disease, Adv. Immunol. 121 (2014) 91–119.
[48] E.M. Hill-Burns, J.W. Debelius, J.T. Morton, W.T. Wissemann, M.R. Lewis, Z.D. Wallen, S.D. Peddada, S.A. Factor, E. Molho, C.P. Zabetian, R. Knight, H. Payami, Parkinson's disease and Parkinson's disease medications have distinct signatures of the gut microbiome, Mov. Disord. 32 (2017) 739–749.
[49] M. Bernardeau, M.J. Lehtinen, S.D. Forssten, P. Nurminen, Importance of the gastrointestinal life cycle of Bacillus for probiotic functionality, J. Food Sci. Technol. 54 (2017) 2570–2584.
[50] H.A. Seddik, F. Bendali, F. Gancel, I. Fliss, G. Spano, D. Drider, Lactobacillus plantarum and its probiotic and food potentialities, Probiotics Antimicrob. Proteins 9 (2017) 111–122.
[51] X.M. Luo, M.R. Edwards, Q. Mu, Y. Yu, M.D. Vieson, C.M. Reilly, S.A. Ahmed, A.A. Bankole, Gut microbiota in human systemic lupus erythematosus and a mouse model of lupus, Appl. Environ. Microbiol. 84 (2018).
[52] F. Pinero, M. Vazquez, P. Bare, C. Rohr, M. Mendizabal, M. Sciara, C. Alonso, F. Fay, M. Silva, A different gut microbiome linked to inflammation found in cirrhotic patients with and without hepatocellular carcinoma, Ann. Hepatol. 18 (2019) 480–487.
[53] H. Ma, B. Zhang, Y. Hu, J. Wang, J. Liu, R. Qin, S. Lv, S. Wang, Correlation analysis of intestinal redox state with the gut microbiota reveals the positive intervention of tea polyphenols on hyperlipidemia in high fat diet fed mice, J. Agric. Food Chem. 67 (2019) 7325–7335.
[54] J.K.Y. Tse, Gut microbiota, nitric oxide, and microglia as prerequisites for neurodegenerative disorders, ACS Chem. Neurosci. 8 (2017) 1438–1447.
[55] A. Paix, D. Antoni, W. Waissi, M.P. Ledoux, K. Bilger, L. Fornecker, G. Noel, Total body irradiation in allogeneic bone marrow transplantation conditioning regimens: a review, Crit. Rev. Oncol. Hematol. 123 (2018) 138–148.
[56] S.K. Seung, D.A. Larson, J.M. Galvin, M.P. Mehta, L. Potters, C.J. Schultz, S.V. Yajnik, A.C. Hartford, S.A. Rosenthal, American college of radiology (ACR) and American society for radiation oncology (ASTRO) practice guideline for the performance of stereotactic radiosurgery (SRS), Am. J. Clin. Oncol. Canc. Clin. Trials 36 (2013) 310–315.